APPLIED AND ENVIRONMENTAL MICROBIOLOGY, Feb. 2007, p. 718–729 Vol. 73, No. 3
0099-2240/07/$08.00+0 doi:10.1128/AEM.01532-06

Shewanella oneidensis MR-1 Fluxome under Various Oxygen Conditions▽†

Yinjie J. Tang,[1,3]‡ Judy S. Hwang,[1,2]‡ David E. Wemmer,[1,2,4] and Jay D. Keasling[1,3,5]*

Physical Biosciences Division, Lawrence Berkeley National Laboratory, Berkeley, California 94720,[1] and Biophysics Graduate Group[2] and Departments of Chemical Engineering,[3] Chemistry,[4] and Bioengineering,[5] University of California, Berkeley, California 94720

Received 5 July 2006/Accepted 1 November 2006

The central metabolic fluxes of *Shewanella oneidensis* MR-1 were examined under carbon-limited (aerobic) and oxygen-limited (microaerobic) chemostat conditions, using ^{13}C-labeled lactate as the sole carbon source. The carbon labeling patterns of key amino acids in biomass were probed using both gas chromatography-mass spectrometry (GC-MS) and ^{13}C nuclear magnetic resonance (NMR). Based on the genome annotation, a metabolic pathway model was constructed to quantify the central metabolic flux distributions. The model showed that the tricarboxylic acid (TCA) cycle is the major carbon metabolism route under both conditions. The Entner-Doudoroff and pentose phosphate pathways were utilized primarily for biomass synthesis (with a flux below 5% of the lactate uptake rate). The anaplerotic reactions (pyruvate to malate and oxaloacetate to phosphoenolpyruvate) and the glyoxylate shunt were active. Under carbon-limited conditions, a substantial amount (9% of the lactate uptake rate) of carbon entered the highly reversible serine metabolic pathway. Under microaerobic conditions, fluxes through the TCA cycle decreased and acetate production increased compared to what was found for carbon-limited conditions, and the flux from glyoxylate to glycine (serine-glyoxylate aminotransferase) became measurable. Although the flux distributions under aerobic, microaerobic, and shake flask culture conditions were different, the relative flux ratios for some central metabolic reactions did not differ significantly (in particular, between the shake flask and aerobic-chemostat groups). Hence, the central metabolism of *S. oneidensis* appears to be robust to environmental changes. Our study also demonstrates the merit of coupling GC-MS with ^{13}C NMR for metabolic flux analysis to reduce the use of ^{13}C-labeled substrates and to obtain more-accurate flux values.

Shewanella oneidensis MR-1 (ATCC 70050) is a gram-negative, facultative anaerobe that was isolated from lake sediment (35). *S. oneidensis* bacteria are capable of utilizing many carbon sources, including lactate, acetate, pyruvate, and some amino acids. Moreover, they are capable of reducing a variety of electron acceptors besides oxygen, including Fe(III), Mn(IV), sulfur, nitrate, and fumarate (26). There have been extensive studies of this strain, focused primarily on its versatile respiration and its potential to engage in cometabolic bioremediation of toxic metals (17, 18, 34, 36, 37).

Recently, the complete *S. oneidensis* genome was sequenced and annotated. Furthermore, key phenotypic and molecular characteristics have been identified (13). The central carbon metabolism of *S. oneidensis* under both aerobic and anaerobic conditions has been investigated using enzyme assays and genome information (11, 26, 27), and there are several unusual features (26, 42). First, a serine pathway is proposed to be active under anaerobiosis in *S. oneidensis* due to the detection of high levels of hydroxypyruvate reductase, which is the key enzyme involved in serine metabolism. Second, *S. oneidensis* shares some metabolic features with nonfermentative pseudomonads, such as utilization of the Entner-Doudoroff (ED) pathway instead of the Embden-Meyerhof-Parnas (EMP) pathway for the oxidation of glucose. Third, because the tricarboxylic acid (TCA) cycle might be truncated under oxygen-limited conditions, the glyoxylate shunt might be present to synthesize TCA cycle intermediates. However, these features have not been rigorously verified using ^{13}C tracer experiments, and very little is known about the actual balances of intracellular metabolic fluxes under different oxygen conditions. Metabolic flux analysis is necessary to provide a detailed physiological characterization of *S. oneidensis* MR-1 and may be important for improving its metal reduction ability through rational metabolic engineering or by stimulating metal reduction in the environment through the addition of growth supplements and electron donors.

^{13}C isotopomer analysis is a powerful approach for mapping intracellular fluxes. By feeding a ^{13}C-labeled carbon source to the cells, the labeling pattern of the primary metabolites, often the amino acids, can be measured. Based on these isotopomer data and the biochemical network of *S. oneidensis* MR-1, a metabolic pathway model can quantify the rates of intracellular reactions (16). In our study, labeling patterns of amino acids were analyzed by both nuclear magnetic resonance (NMR) spectroscopy and gas chromatography-mass spectrometry (GC-MS). The advantage of NMR is that it provides positional information about the labels in the isotopomers even though detection sensitivity is low (2). GC-MS is a more sensitive detection method and determines what fraction of a particular molecule or molecular fragment contains a specific number of labels (38). By combining GC-MS and NMR data, a complete picture of the isotopomer distribution in amino acids can be

* Corresponding author. Mailing address: Berkeley Center for Synthetic Biology, University of California, Berkeley, CA 94720. Phone: (510) 642-4862. Fax: (510) 495-2630. E-mail: Keasling@berkeley.edu.

† Supplemental material for this article may be found at http://aem.asm.org/.

‡ These authors contributed equally to the work.

▽ Published ahead of print on 10 November 2006.

obtained. The main goal of this study was to determine the fluxes through key metabolic pathways in *S. oneidensis* MR-1 under aerobic and microaerobic conditions. The determination of fluxes was accomplished in three steps: (i) the cells were grown in defined medium with ^{13}C-labeled lactate as the sole carbon source, (ii) the labeling patterns in key amino acids of the total protein hydrolysate were characterized using both GC-MS and NMR, and (iii) a flux calculation algorithm was used to quantify the central metabolic pathways. Two sets of conditions were probed to determine the flux distribution, carbon limitation (dissolved oxygen [DO] > 70%) and oxygen limitation (DO < 10%). The results not only widen our understanding of *Shewanella* metabolism but also demonstrate a powerful approach for investigating metabolic flux analysis using both GC-MS and NMR techniques.

MATERIALS AND METHODS

Culture conditions. *S. oneidensis* MR-1 was purchased from the American Tissue Culture Center (ATCC 70050) and was stored at −80°C prior to use. All cultures used the modified MR-1 defined medium (31) (see the supplemental material). The lactate used was either [3-^{13}C]sodium L-lactate (98%; Cambridge Isotope), [1-^{13}C]sodium L-lactate (99%; Cambridge Isotope), or a mixture of 10% [$^{13}C_3$]sodium L-lactate (99%; Cambridge Isotope) and 90% unlabeled sodium lactate (Fisher).

Fermentations were carried out in a 1-liter New Brunswick Bioflo 110 fermentor. The off-gas composition was analyzed using a mass spectrometer (Thermo Onix). The inoculum was prepared in LB medium in shake flasks overnight (optical density at a wavelength of 600 nm [OD_{600}] > 1.5). Fermentations were started with a 1% inoculated volume for optimal growth kinetics. After three residence periods in continuous mode, the amount of LB remaining was very small (<0.05%). The reactor temperature was maintained at 30°C. The working volume in the bioreactor was kept at 500 ml, and agitation was set at 300 rpm. For the carbon-limited condition, 30 mM [3-^{13}C]L-lactate was used, and the dilution rate was set to 0.079 h^{-1} in order to keep the DO level over 70% during continuous culture. For the oxygen-limited condition, 50 mM lactate composed of 10% [$^{13}C_3$]L-lactate and 90% unlabeled lactate was used. The dilution rate was set to 0.10 h^{-1}, and the DO level was controlled below 10% during continuous culture. In both experiments, the continuous culture was started after 15 h of batch culture and continued for three generations. During both continuous cultures, the medium was controlled at pH ~8, and the final OD_{600} was around 1. ^{13}C-labeled biomass was sampled after three generation periods for biomass composition analysis and isotopomer measurements. For shake flask experiments, cells were grown in 10 ml of three differently labeled lactate media (shaking speed = 200 rpm): [3-^{13}C]L-lactate, [1-^{13}C]L-lactate, or [$^{13}C_3$]lactate (10% [$^{13}C_3$]L-lactate with 90% unlabeled lactate). The final concentration of lactate was 30 mM. The MR-1 inoculum was prepared in labeled, modified MR-1 defined medium, and 2% of the final culture volume was inoculated into the same medium in shake flasks. The biomass in shake flasks was harvested in the mid-exponential growth phase (OD_{600} ~ 0.5).

Analytical methods for extracellular metabolites and biomass compositions. Cell growth was monitored by measuring the OD_{600}. The harvested culture was centrifuged at 4,800 × *g* and 4°C for 20 min and lyophilized overnight. The dried biomass was weighed and used for fatty acid quantification using fatty acid methyl ester analysis (33) (Microbial ID, Newark, DE). The total protein concentration was determined by the Bradford protein assay (catalog no. 500-0006; Bio-Rad). The concentrations of lactate, acetate, pyruvate, and succinate in the medium were measured using enzyme kits (r-Biopharm, Darmstadt, Germany), and lactate, pyruvate, and acetate were also quantified using one-dimensional (1D) ^{1}H presaturation NMR spectra. The relaxation delay between scans was set to 20 s, and 100 μM sodium 3-trimethylsilylpropionate (TSP) added to the sample was used as the reference compound for quantification. The reported results are the averages for both enzymatic and NMR measurements.

All measurement methods for biomass constituents (protein, carbohydrates, RNA, and DNA) were taken from previously reported protocols (4, 15, 16). Total protein content was determined using the Bradford method, total carbohydrate content was determined by the phenol reaction, RNA was assayed through a reaction involving orcinol, and DNA was obtained through the colorimetric procedure that involves the reaction of DNA with diphenylamine in a mixture of perchloric acid. Glucose, pure *Escherichia coli* RNA (catalog no. 7940; Ambion), and deoxyribose were used as standards for the carbohydrate, RNA, and DNA measurements, respectively. Quantification of amino acids in protein was performed by the Molecular Structure Facility (University of California—Davis).

Gas chromatography-mass spectrometry. Before measurement of amino acid-labeling patterns in cellular protein, a 10-ml culture was harvested and centrifuged down at 8,000 × *g*. The cell pellets were washed once with 0.9% NaCl and then suspended in 1 ml of sterile nanopure water and sonicate, using the microtip for 3 min with a 3-s-on/1-s-off cycle. The proteins from the resulting lysate were precipitated using trichloroacetic acid, washed with cold acetone two times, and then hydrolyzed in 6 M HCl at 100°C for 24 h. GC-MS was carried out using a gas chromatograph (DB5 column, HP6890 series; Agilent Inc.) equipped with a mass spectrometer (5973 Network; Agilent Inc.). GC-MS samples were prepared in 100 μl of tetrahydrofuran (THF) and 100 μl of *N*-(*tert*-butyldimethylsilyl)-*N*-methyl-trifluoroacetamide (Sigma-Aldrich). All samples were derivatized in a water bath at 65 to 80°C for 1 h. Two types of positively charged species were clearly observed by MS in this study: unfragmented molecules, designated $[M-57]^+$, and fragmented molecules that had lost one carboxyl group, designated $[M-159]^+$. For the former, M is the total molecular mass of the derivatized hydrolysate component, and 57 indicates the loss of 57 mass units, e.g., a *tert*-butyl group. For amino acids that contain two carboxyl groups, the loss of the α carboxyl group is strongly favored because the amine group on the β-carbon allows the formation of an entropically stable fragment (6, 12). The natural abundance of isotopes, including ^{13}C (1.13%), ^{18}O (0.20%), ^{29}Si (4.70%), and ^{30}Si (3.09%) (Si occurs in amino acids derivatized for gas chromatography separation), changes the mass isotopomer spectrum. These changes were corrected using a published algorithm before the data were used for calculating the label distribution (14).

^{13}C NMR sample preparation and analysis. An aliquot (50 ml) of culture was harvested by centrifugation at 5,000 × *g* for 20 min at 4°C. The cell pellet was washed twice with 20 mM NaH_2PO_4 (in D_2O) (pH 7) buffer. Washed pellets were resuspended in the same buffer, and the cells were disrupted by sonication. The cells were sonicated four or five times, for 15 to 20 seconds each time, at sonication power level 3 on a model 300 Misonix sonicator (Misonix Inc.). Cell debris was removed by centrifugation at 11,250 × *g* for 30 min at 4°C. Cellular protein in the supernatant was then hydrolyzed in 6 M HCl by incubation at 95 to 100°C for 24 h. The hydrolysate was filtered through a 0.22-μm-pore-size filter and lyophilized. The dried material was dissolved in 700 μl of 20 mM deuterium chloride in D_2O, filtered through a 0.22-μm-pore-size filter, and used for the NMR measurements.

Proton-detected 2D ^{13}C-^{1}H heteronuclear single-quantum correlation spectroscopy spectra were collected with the pulse sequence and parameters described in reference 5. The spectra were recorded at a ^{1}H frequency of 600 MHz on a Bruker DRX 600 spectrometer and analyzed with the software programs NMRPipe and NMRDraw (5). For each sample, two spectra were taken: one for the aliphatic resonances, with the ^{13}C carrier set to 43 ppm, and the other for the aromatic resonances, with the ^{13}C carrier set to 125 ppm. The data sizes were 3,500 by 1,024 complex points. The acquisition times were 686 ms (maximum indirect evolution time [t_{1max}]) and 128 ms (maximum acquisition time [t_{2max}]). The relaxation delay between scans was set to 2.2 to 2.3 s, and the spectra were collected at 25°C for all 2D NMR experiments. The relative distributions of the isotopomers were determined from the intensities of the individual multiplet components in ^{13}C-^{13}C scalar-coupled multiplets (30).

Algorithm for flux calculation and isotopomer modeling. Central biochemical pathways for *S. oneidensis* MR-1 were selected based on the Internet-accessible genome database MicrobesOnline (1). The complete list of key reactions in the model is given in the supplemental material, and the reaction network is shown in Fig. 1. The pathway map includes the TCA cycle (including the glyoxylate shunt), C_1 metabolism, the ED pathway, and the pentose phosphate (PP) pathway. The shaded boxes in Fig. 1 represent the biomass pool containing key amino acids for which the isotopomer distributions were measured by GC-MS and NMR. There are 36 free fluxes to be determined in the pathway map. The extracellular fluxes, v1 and v6, were directly measured using enzymatic methods. An isotopomer solution algorithm was developed using MATLAB 6.0 (The Mathworks, Natick, MA). To search for a global solution, an iterative procedure, which consisted of the following steps, was used. (i) A set of initial guesses for all fluxes was inserted into the solution algorithm. The speed of converging to a global solution depends on the guess for the initial value. The starting guess for independent fluxes was coarsely based on MR-1 biomass composition or fluxes reported previously for the well-known microorganism *Escherichia coli*. After each round of iteration, a set of improved guessed fluxes was found and then used as a new search point. The complete fluxes in the pathway map were solved using the reaction stoichiometric matrix (29). (ii) Concepts of atom mapping

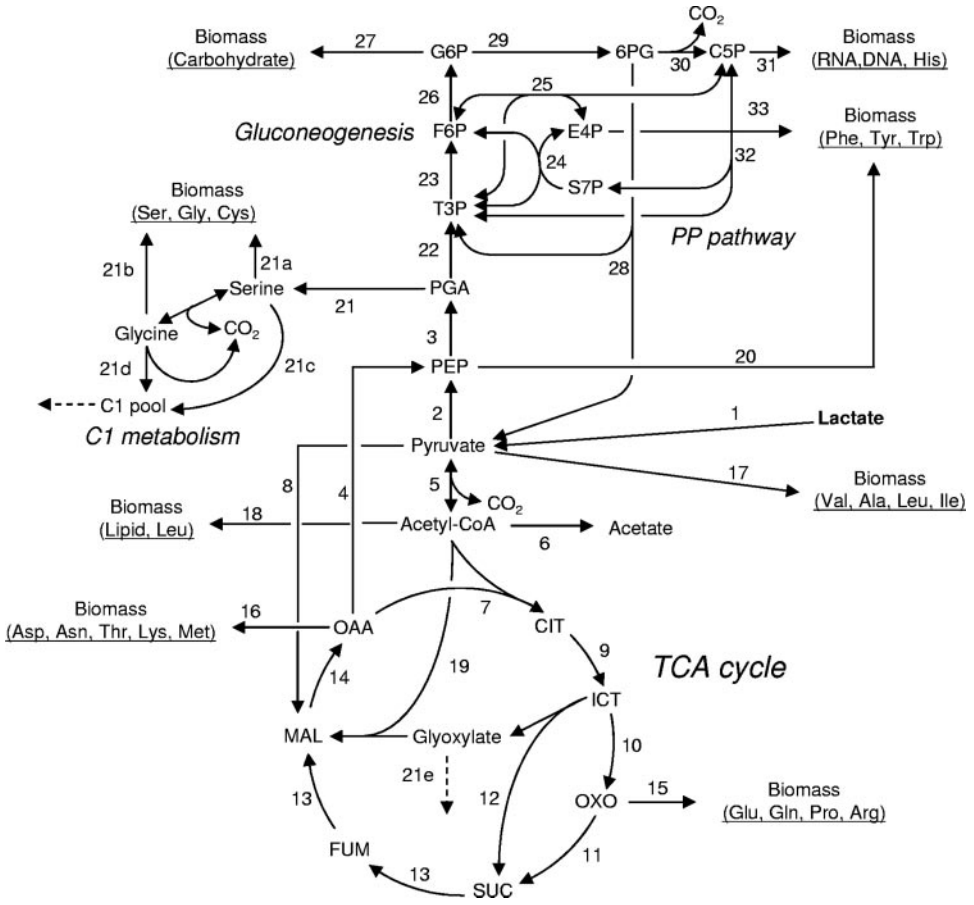

FIG. 1. Pathways of lactate metabolism in *S. oneidensis* MR-1. Reaction 21e (glyoxylate → glycine) is not present in the annotated genome sequence. The amino acids used for isotopomer models are indicated in parentheses. The numbers represent the reactions included in the model (corresponding to the reactions listed in the supplemental material). Abbreviations: 6PG, 6-phosphogluconate; Acetyl-CoA, acetyl-coenzyme A; C1, 5,10-Me-THF; C5P, ribose-5-phosphate (or ribulose-5-phosphate or xylulose-5-phosphate); CIT, citrate; E4P, erythrose-4-phosphate; F6P, fructose-6-phosphate; G6P, glucose-6-phosphate; ICT, isocitrate; MAL, malate; OAA, oxaloacetate; OXO, 2-oxoglutarate; PEP, phosphoenolpyruvate; PGA, 3-phosphoglycerate; PYR, pyruvate; S7P, sedoheptulose-7-phosphate; SUC, succinate; T3P, triose-3-phosphate.

matrices and isotopomer mapping matrices were used in an iterative scheme to calculate the steady-state isotopomer distributions in the intracellular metabolite pools, and these were transformed to MS and NMR data (24, 25). The simulated MS and NMR data for isotopomer distributions of proteinogenic amino acids were compared to the experimental results. (iii) For each search point, the local optimal solution was found using the Nelder-Mead method (via the fminsearch function in MATLAB). (iv) A simulated annealing strategy was used to obtain an optimal global solution. First, an optimal local solution was perturbed by taking a finite amplitude step away from it, and then steps 1 to 4 were repeated to see whether a better solution could be obtained. The global search stopped when the objective function could not be further minimized (20). The objective function is defined as follows:

$$\varepsilon(v_n) = \sum_{i=1}^{a}\left(\frac{M_{i,m} - M_{i,c}(v_n)}{\delta_i}\right)^2 + \sum_{j=1}^{b}\left(\frac{N_{j,m} - N_{j,c}(v_n)}{\delta'_j}\right)^2 \quad (1)$$

where v_n represents the unknown fluxes to be optimized in the program based on amino acids i to a (as measured by GC-MS) or j to b (as measured by NMR), $M_{i,m}$ represents the measured MS data, and $M_{i,c}$ represents the corresponding model-simulated values. $N_{i,m}$ represents the measured NMR data, and $N_{i,c}$ represents the corresponding model-simulated values. δ and δ' are the experimental errors for measured MS and NMR data, respectively. To save computational time, biomass fluxes were constrained based on the uncertainty of the measurement. The confidence intervals for the calculated fluxes can be estimated by Monte Carlo methods (20): (i) the measured data were perturbed randomly within measurement noise; (ii) the optimization routine described above was used to estimate the new flux distribution after each perturbation; and (iii) after over 100 simulated measured data sets were tested, the error bounds on the flux distributions resulting from errors in all measurements were obtained.

All reactions could be potentially reversible and make the system highly underdetermined (29). Several reactions (v4, v5, v11, v8, v12, and v21) were considered to be reversible because they have the most significant impact on the isotopomer distribution (2, 43). The reversible reactions are characterized by their net flux, v_i, and their exchange flux, v_i^{exch}. The net flux is defined as the difference between forward and backward fluxes. The exchange flux, v_i^{exch}, is the smaller of the forward and backward fluxes. Equation 2 rescales v_i^{exch}(possible value range, 0 to ∞) to the exchange coefficient $exch_i$, which has a finite range (0 to 1) (39):

$$v_i^{exch} = \beta \frac{exch_i}{1 - exch_i} \quad (2)$$

where β is a constant of the order of magnitude of v_i. In our study, a value of 1 was assigned to β. Exchange coefficients are limited to values between 0 and 0.95 in order to improve the speed of convergence.

Sensitivity test of isotopomer model. The flux calculation is based on tracing the path of ^{13}C from labeled carbon substrate to metabolites in the pathway network. Singly labeled or fully labeled ^{13}C substrate (often 10 to 20%) can be used for tracer experiments in flux analysis (8). Although the labeling pattern of substrate should not affect the actual flux distributions, it may affect the sensitivity of isotope data to model calculations (2, 40). Some studies have shown that the ED and PP pathways are particularly well resolved using singly labeled carbon substrate, whereas the fully labeled carbon substrate is ideal for reactions

in the TCA cycle because information from ^{13}C-^{13}C connectivity can be obtained (9). Other studies have shown that the use of a mixed labeling pattern (containing certain percentages of unlabeled, fully labeled, and doubly labeled substrate) may be the most useful for ascertaining metabolic fluxes (2). However, most studies on the sensitivity of isotopomer distributions have used glucose as the carbon source and focused on GC-MS as the only measurement technique. To avoid a potential bias in calculated fluxes, our study utilized two different labeling strategies: 10% fully labeled lactate for the oxygen-limited chemostat and 98% singly labeled lactate for the carbon-limited chemostat. To minimize the cost of labeled lactate for fermentations, these two types of labeled lactate medium were also used in shake flask cultures to provide an additional comparison for sensitivity analysis.

After global solutions are obtained for flux distributions of cells grown under different culture conditions, a sensitivity test is necessary to check the reliability of the model results and to estimate the confidence interval for the calculated fluxes. The sensitivity coefficient, which reflects the sensitivity of mass distribution upon changes in fluxes and exchange coefficients, is defined as follows:

$$S_{ij} = \frac{\partial I_i}{\partial v_j} \approx \frac{I'_i - I_i}{v'_j - v_j} \quad (3)$$

where I_i represents the isotopomer data for the amino acid (i) and v_j represents the flux or exchange coefficient (j) (2). Since the analytical expression is difficult to derive, an approximation has to be made. After the global solution with the best-fitted isotopomer data (I_i) is found, the optimized flux distribution (v_j) is then perturbed with a small change in its independent fluxes and exchange coefficients. The resulting new flux distribution (v'_j) predicts a new set of isotopomer data (I'_i), and equation 3 can be applied to estimate the sensitivity of the model.

RESULTS

Aerobic chemostat and shake flask cultivations. Continuous cultivation was performed under two conditions: carbon limitation (30 mM lactate; DO > 70%) and oxygen limitation (50 mM lactate; DO < 10%). Cell growth, lactate consumption, and acetate production were measured during the cultivation (Fig. 2). During the batch phases under both conditions, some of the lactate was converted to acetate. Under the carbon-limited condition with a low growth rate ($D = 0.079\ h^{-1}$), neither lactate nor acetate was detected in the effluent of the continuous culture, while under the oxygen-limited condition with a higher growth rate ($D = 0.10\ h^{-1}$), 17.5 mM acetate was detected in the effluent of the continuous culture. The CO_2 concentration in the off-gas remained constant after two generations. Similar final OD_{600} and biomass concentration were the basis for our comparison between these two chemostat cultures (Table 1). In parallel with the continuous culture, *S. oneidensis* MR-1 was grown in shake flasks with labeled lactate. The profiles of growth, lactate consumption, and acetate production were similar to those for the batch phase of chemostat cultures (data not shown). The observed doubling time in defined medium was approximately 4 h, which was equivalent to a growth rate of $0.17\ h^{-1}$. The results also reflect the growth kinetics of *S. oneidensis* MR-1: a high growth rate and low dissolved oxygen level enhanced acetate production under aerobic conditions (32).

Biomass composition analysis. Analysis of biomass composition not only helps clarify the biosynthetic kinetics but also provides the initial guesses for some intracellular fluxes in our calculation algorithm. The biomass compositions of *S. oneidensis* MR-1 grown under both shake flask and chemostat conditions are similar to those of *E. coli*, even though *E. coli* was grown on a different carbon source under different growth conditions (Table 2). The RNA and DNA fractions of the biomass from the shake flask cultures were relatively similar to those observed in the chemostat cultures, whereas the fatty acid fraction of the shake flask cultures was much less than that of the chemostat cultures. The undetermined weight fraction was probably soluble metabolites, residual salts, and bound water that was not completely removed from the biomass by lyophilization. Fatty acid methyl ester analysis showed that the fatty acid profile was dominated by even-numbered fatty acids (see Table S1 in the supplemental material). The amino acid mole fractions from cellular protein were very similar in the two chemostat cultures and the shake flask cultures (see Fig. S1 in the supplemental material). This may indicate that even though specific proteins are different under the two conditions, the amino acid fractions in total proteins do not change under those growth conditions.

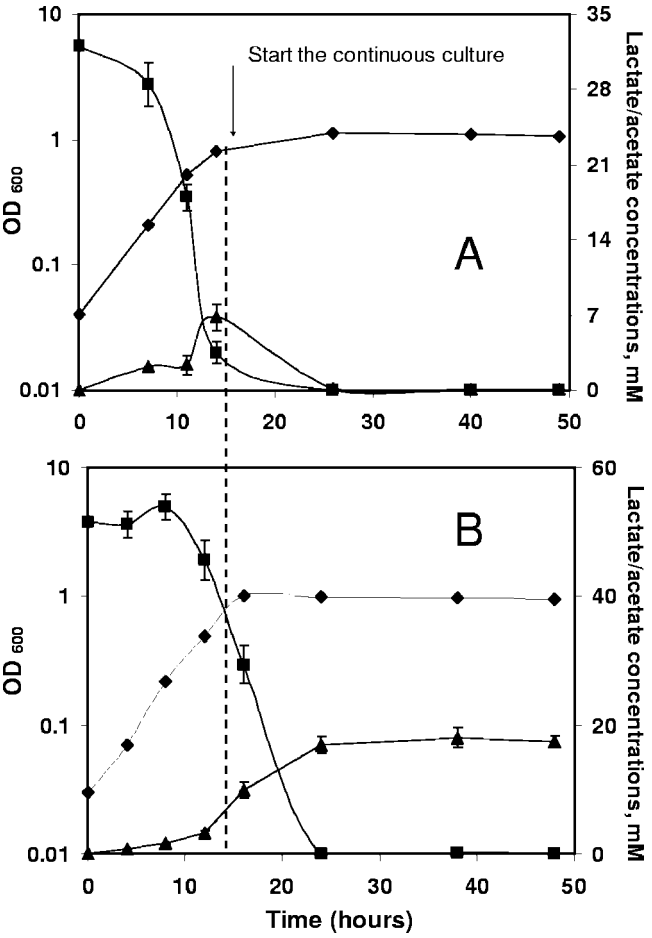

FIG. 2. Time courses of biomass growth (◆), lactate concentration (■), and acetate secretion (▲) in chemostat experiments under carbon-limited conditions (A) and oxygen-limited conditions (B). All data points have error bars representing the errors in the measurement; some error bars are not visible due to the very small measurement errors.

Isotopomer distribution profiles. Although NMR and MS analyses have both been used successfully in previous work, the latter was thought to be high throughput and more sensitive (≤2% errors), with comparatively low cost (22). Applying GC-MS to separate the derivatized protein hydrolysate gave chromatographic peaks for 15 proteinogenic amino acids (ar-

TABLE 1. Comparison of cultivation parameters of *S. oneidensis* MR-1 cultures[a]

Culture	Growth or dilution rate (h^{-1})	Sampling OD_{600}	DO level (%)	Biomass concn (g/liter)	Lactate remaining (mM)	Acetate excreted (mM)	Pyruvate excreted (mM)	Lactate consumption rate (mM/g DCW/h)	CO_2 formation rate (mM/g DCW/h)
Shake flask ($n = 5$)	0.17	~0.5	ND[b]	0.26 ± 0.04	13.5 ± 1.1	3.2 ± 0.6	~0.5	7.2 ± 0.7	ND
Chemostat									
Oxygen limited	0.10	~1.0	70	0.63 ± 0.05	~0.3	17.5 ± 0.9	~0.1	7.9 ± 0.6	13.7 ± 1.5
Carbon limited	0.079	~1.0	0 to ~10	0.58 ± 0.03	~0	~0	~0	4.1 ± 0.3	9.8 ± 1.2

[a] DCW, dry cell weight.
[b] ND, not determined. Dissolved oxygen dropped during the exponential growth phase in shake flasks (31).

ginine, asparagine, cysteine, glutamine, and tryptophan could not be determined). The possible alternative routes for leucine and isoleucine synthesis suggested by the MR-1 genome information are complicated, and the MS peaks for both amino acids ($[M-57]^+$) were overlapped by other signals, so their isotopomer distributions were not considered in the model calculation. Consistent with assumed amino acid biosynthesis pathways, several amino acid pairs derived from the same precursor, such as proline and glutamate (from precursor oxoglutarate), threonine and aspartate (from precursor oxaloacetate), and tyrosine and phenylalanine (from precursors phosphoenolpyruvate [PEP] and erythrose-4-phosphate), had similar isotopomer patterns from both MS and NMR measurements (29). This redundant isotopomer information could be utilized to estimate the experimental errors (8).

Flux analysis requires the pools of intracellular metabolites to be in an isotopomeric steady state. Although flux analysis is best studied in the physiological steady state by continuous bioreactor culture, many studies have shown that a (quasi) steady state can also be achieved during the exponential growth phase (or even at stationary phase) in batch culture (7, 23, 28). For a convenient and less expensive approach to test the reproducibility of isotopomer distribution determinations, biomass was also cultured in 10-ml shake flasks, using the same medium as for the chemostat cultures. The isotopomer distributions of key amino acids from shake flask and chemostat cultures had relatively similar profiles, with less than 10% difference (fragment $[M-57]^+$ in Table 3 and fragment $[M-159]^+$ in Table S2 in the supplemental material). There were larger differences (10 to 15%) in the isotopomer ratios of the mass fragments of phenylalanine between the carbon-limited chemostat and shake flask cultures.

The ^{13}C abundance for individual carbon positions is helpful for identifying reactions in the metabolic network and for providing additional constraints for the isotopomer model. In this study, the labeling patterns of the key amino acids in the hydrolysate were analyzed by 2D ^{1}H-^{13}C correlation spectroscopy NMR. In the indirectly detected ^{13}C dimension, multiplets arise from scalar spin-spin coupling between directly linked ^{13}C carbon spins. For the α carbon of a fractionally labeled amino acid, up to four different patterns of multiplets (isotopomers) may be observed. Based on the ratios of peak intensities, the relative populations of isotopomers can be determined (29). However, because of some overlap in multiplet peaks and signals arising only from the natural abundance of ^{13}C, estimations of the isotopomer distributions were not always unique. Therefore, model calculations considered only the most reliable NMR data on nine amino acids for the isotopomer model analysis, mainly from α and β carbons (Table 4).

Flux calculation and model reliability test. The isotopomer model provided flux distributions for both chemostat cultures and shake flask cultures. The lactate carbon flux (taken to be 100%) is split into two branches at the pyruvate: one flows toward the TCA cycle, and the other flows toward the PP and ED pathways (Fig. 3). For the carbon-limited condition, 61% of the substrate entered the TCA cycle via acetyl-coenzyme A (acetyl-CoA) condensing with oxaloacetate. For the microaerobic condition, the TCA cycle was weakened, as the relative carbon flux through the TCA cycle dropped to 47%; approximately 35% of the lactate was converted into acetate. Additionally, the calculations indicate that some fluxes might be highly reversible, such as the serine metabolism route. The reversibility of the serine metabolism route could alter the mass distribution of serine and glycine significantly. Although all the reactions in the PP pathway were thought to be reversible, the total fluxes through the PP reactions were small (<4%

TABLE 2. Comparison between biomass compositions of *S. oneidensis* MR-1 and *E. coli*

Species and culture	Value (%) for:					
	Protein	RNA	DNA	Fatty acids	Carbohydrate	Other
S. oneidensis MR-1						
Shake flask[a]	51 ± 5	16.2 ± 1.9	2.7 ± 0.4	9.2 ± 1.2	12 ± 2	~8.9
Chemostat						
Oxygen limited	48 ± 3	14.0 ± 2.5	2.5 ± 0.4	15.1 ± 1.2	11 ± 3	~9.4
Carbon limited	48 ± 4	13.6 ± 2.3	2.1 ± 0.5	14.8 ± 0.8	10 ± 3	~9.5
E. coli[b]	52	16	3	9.1 (lipid fraction)	17	3 (ash wt)

[a] Lactate (30 mM) was used.
[b] Glucose medium under aerobic culture. Reported values for *E. coli* are adapted from reference 29.

TABLE 3. Measured and predicted mass fragment $[M-57]^+$ distributions of TBDMS-derivatized amino acids from *S. oneidensis* MR-1 hydrolysates[a]

Amino acid(s) and ion	Measured (predicted) value for indicated culture group			
	Chemostat, carbon limited	Shake flask, 3-^{13}C[b]	Chemostat, oxygen limited	Shake flask, 10% $^{13}C_3$[c]
Ala				
M0	0.01 (0.02)	0.02 ± 0.01	0.90 (0.89)	0.89 ± 0.01
M1	0.98 (0.97)	0.97 ± 0.01	0 (0.01)	0 ± 0
M2	0 (0.01)	0.0 ± 0	0.01 (0)	0.01 ± 0
Val				
M0	0.01 (0.01)	0 ± 0	0.79 (0.81)	0.81 ± 0
M1	0.03 (0.02)	0.02 ± 0.01	0.01 (0.01)	0.01 ± 0
M2	0.92 (0.95)	0.92 ± 0.02	0.10 (0.09)	0.10 ± 0.01
M3	0.01 (0.01)	0.01 ± 0.01	0.09 (0.09)	0.08 ± 0
Asp/Asn				
M0	0 (0)	0 ± 0	0.75 (0.76)	0.77 ± 0.02
M1	0.20 (0.18)	0.20 ± 0.02	0.15 (0.13)	0.13 ± 0.02
M2	0.40 (0.40)	0.39 ± 0.01	0.07 (0.09)	0.05 ± 0.02
M3	0.40 (0.41)	0.41 ± 0.02	0.03 (0.02)	0.06 ± 0.02
Met				
M0	0.01 (0)	0.01 ± 0	0.64 (0.65)	0.66 ± 0.03
M1	0.04 (0.05)	0.05 ± 0.01	0.21 (0.21)	0.22 ± 0.02
M2	0.22 (0.24)	0.24 ± 0.02	0.12 (0.10)	0.09 ± 0.02
M3	0.39 (0.40)	0.38 ± 0.03	0.03 (0.04)	0.03 ± 0.01
Ser				
M0	0.07 (0.06)	0.06 ± 0.02	0.86 (0.87)	0.85 ± 0
M1	0.72 (0.72)	0.74 ± 0.03	0.07 (0.04)	0.06 ± 0.01
M2	0.16 (0.16)	0.15 ± 0.02	0.03 (0.02)	0.03 ± 0
Gly				
M0	0.68 (0.69)	0.69 ± 0.02	0.88 (0.87)	0.90 ± 0.01
M1	0.21 (0.23)	0.22 ± 0.02	0.04 (0.06)	0.01 ± 0
Glu/Gln				
M0	0 (0)	0 ± 0	0.70 (0.71)	0.72 ± 0.03
M1	0.01 (0.01)	0.01 ± 0	0.15 (0.14)	0.14 ± 0.01
M2	0.31 (0.30)	0.32 ± 0.02	0.12 (0.13)	0.12 ± 0
M3	0.48 (0.49)	0.48 ± 0.01	0.02 (0.02)	0.02 ± 0
M4	0.18 (0.19)	0.20 ± 0.01	0 (0)	0 ± 0
Phe				
M0	0 (0)	0 ± 0	0.57 (0.55)	0.61 ± 0.05
M1	0 (0)	0 ± 0	0.17 (0.18)	0.12 ± 0.03
M2	0.02 (0.03)	0.01 ± 0.01	0.09 (0.10)	0.08 ± 0.02
M3	0.45 (0.38)	0.61 ± 0.11	0.12 (0.12)	0.14 ± 0.04
M4	0.30 (0.32)	0.19 ± 0.06	0.03 (0.03)	0.02 ± 0.01
M5	0.14 (0.18)	0.09 ± 0.03	0.01 (0.01)	0.02 ± 0.01
His				
M0	0.01 (0)	0 ± 0	0.71 (0.68)	0.73 ± 0.03
M1	0.04 (0.03)	0.05 ± 0.01	0.07 (0.13)	0.04 ± 0.03
M2	0.26 (0.27)	0.27 ± 0.02	0.11 (0.10)	0.11 ± 0
M3	0.50 (0.50)	0.49 ± 0.02	0.09 (0.08)	0.11 ± 0.01
M4	0.11 (0.14)	0.06 ± 0.03	0.01 (0.01)	0 ± 0

[a] The mass distributions of tyrosine and threonine were identical to those of phenylalanine and aspartate, respectively. The measured (predicted) percentages of $^{13}CO_2$ in the total CO_2 are as follows: for the carbon-limited chemostat group, 0.13 (0.14); for the 3-^{13}C shake flask group, not determined; for the oxygen-limited chemostat group, 0.04 (0.03); and for the 10% $^{13}C_3$ shake flask group, not determined. $^{13}CO_2$ fraction is based on off-gas composition.

[b] Shake flask culture at exponential phase with 98% [3-^{13}C]L-lactate (30 mM). Standard deviations for isotopomer data were based on three replicates.

[c] Shake flask culture at exponential phase with a mixture of 10% fully labeled L-lactate and 90% unlabeled lactate (30 mM) ($n = 3$).

TABLE 4. Results for NMR measurement and model prediction of ^{13}C isotopomer distributions of key amino acids from *S. oneidensis* MR-1 hydrolysates

Amino acid and α-carbon fragment	Measured (predicted) value for indicated chemostat group[a]	
	Carbon limited[b]	Oxygen limited
α-Asp		
Cα	0.23 (0.18)	0.37 (0.33)
Cα-Cβ	0.47 (0.49)	0.11 (0.06)
Cα-C═O	0.05 (0.02)	0.42 (0.47)
Cβ-Cα-C═O	0.25 (0.30)	0.10 (0.13)
α-Ser		
Cα	0.17 (0.17)	0.21 (0.19)
Cα-Cβ	0.52 (0.51)	0.06 (0.03)
Cα-C═O	0.07 (0.02)	0.26 (0.28)
Cβ-Cα-C═O	0.25 (0.29)	0.47 (0.50)
α-Gly		
Cα	0.70 (0.68)	0.41 (0.41)
Cα-C═O	0.29 (0.32)	0.59 (0.59)
α-Glu		
Cα	0.25 (0.32)	0.31 (0.32)
Cα-Cβ	0.45 (0.43)	0.15 (0.13)
Cα-C═O	0.06 (0.04)	0.54 (0.51)
Cβ-Cα-C═O	0.24 (0.22)	0.01 (0.04)
α-Phe		
Cα	0.18 (0.17)	0.14 (0.10)
Cα-Cβ	0.51 (0.51)	0.01 (0.01)
Cα-C═O	0.04 (0.02)	0.04 (0.11)
Cβ-Cα-C═O	0.27 (0.29)	0.83 (0.77)
β-Ser		
Cβ	0.81 (0.82)	0.50 (0.49)
Cβ-Cα	0.19 (0.18)	0.50 (0.51)
β-Asp		
Cβ	0.26 (0.32)	0.36 (0.33)
Cβ-Cα	0.41 (0.41)	0.15 (0.13)
Cβ-Cγ	0.07 (0.04)	0.40 (0.47)
Cα-Cβ-Cγ	0.26 (0.23)	0.09 (0.07)
β-Glu		
Cβ	0 (0)	0.72 (0.73)
Cβ-Cα or Cβ-Cγ	0.26 (0.21)	0.28 (0.27)
Cα-Cβ-Cγ	0.73 (0.79)	0 (0.01)
β-Ala		
Cβ	0.96 (0.98)	0.11 (0.10)
Cβ-Cα	0.04 (0.02)	0.89 (0.90)
β-His		
Cβ	NA	0.10 (0.15)
Cβ-Cα	NA	0.90 (0.85)
Cβ-Cγ	NA	0 (0)
α-Ace		
Cα	ND	0.11 (0.10)
Cα-Cβ	ND	0.89 (0.90)

[a] The standard deviation for NMR measurement was 4 to 5%.

[b] NA, natural abundance; ND, not determined.

of the lactate uptake); thus, the reversibility could be neglected in the model in order to reduce computation time (43). Studies have shown that ^{13}C tracer experiments give only crude estimates of some exchange rates (often within 1

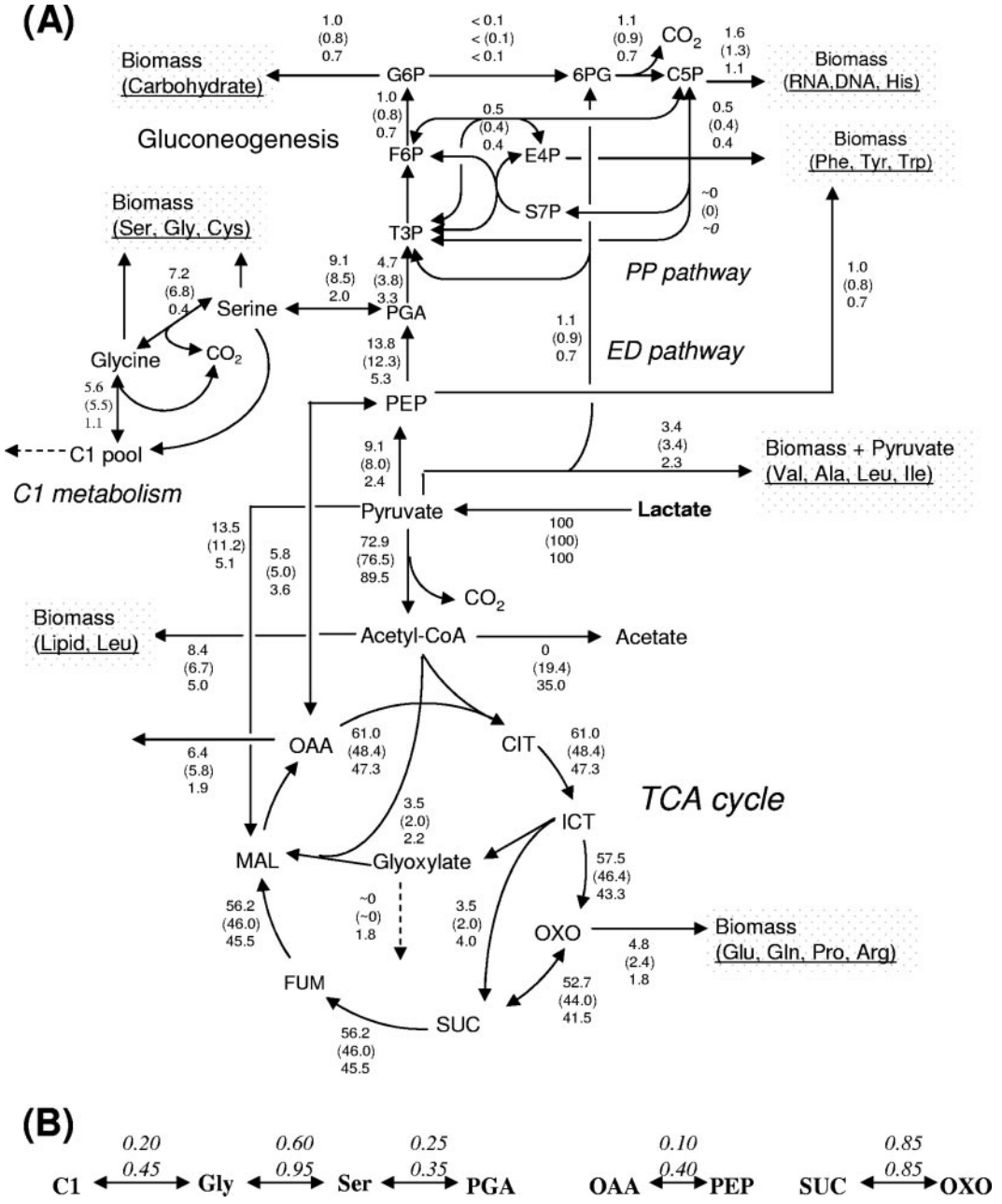

FIG. 3. (A) In vivo flux distribution in the central metabolism of *S. oneidensis* MR-1 under carbon-limited (upper numbers), shake flask (middle numbers, in parentheses), and oxygen-limited (lower numbers) conditions. (B) Exchange coefficients for significant reversible fluxes estimated for carbon-limited (upper numbers) and oxygen-limited (lower numbers) chemostat cultures. OAA, oxaloacetate; MAL, malate; OXO, 2-oxoglutarate; PGA, 3-phosphoglycerate; SUC, succinate; CIT, citrate; FUM, fumarate.

order of magnitude); thus, there is no need to consider the reversibility of every reaction (25, 41).

The reliability of model results was checked using sensitivity coefficients, which are a concept similar to the model objective function (equation 1) (43). By making small changes to specific optimized fluxes, the resulting new fluxes predicted the changes in the isotopomer distributions of specific amino acids. For example, by increasing or decreasing the pyruvate-to-malate flux, the model predicted the change in the isotopomer distributions of Asp and Glu. The absolute values for the sensitivity coefficients were determined, and then the sums of their squares were determined (Table 5). As for singly labeled lactate, the model was sensitive to both GC-MS and NMR data based on the sums of the squared sensitivity coefficients (for GC-MS, 0.00077, and for NMR, 0.00082). On the other hand, the sum of the squared sensitivity coefficients determined using 10% fully labeled lactate (for GC-MS, 0.00007) was 1 order of magnitude lower than that determined using the singly labeled lactate. This indicated that using GC-MS data from 10% fully labeled lactate experiments might produce biased results. However, the model was very sensitive to

TABLE 5. Results for sensitivity test for predicted mass distribution signals (GC-MS $[M-57]^+$ and NMR [α or β carbon]) for aspartate and glutamate upon changes in the futile flux, v8[a]

Amino acid	GC-MS data			NMR data		
	Sensitivity coefficient	3rd carbon labeled[b]	Fully labeled[c]	Sensitivity coefficient	3rd carbon labeled[b]	Fully labeled[c]
Asp	$\left\lvert\frac{\Delta M_0}{\Delta v_8}\right\rvert$	0.0001	0.0041	$\left\lvert\frac{\Delta C\alpha}{\Delta v_8}\right\rvert$	0.013	0.015
	$\left\lvert\frac{\Delta M_1}{\Delta v_8}\right\rvert$	0.0100	0.0057	$\left\lvert\frac{\Delta C\alpha - C\beta}{\Delta v_8}\right\rvert$	0.005	0.008
	$\left\lvert\frac{\Delta M_2}{\Delta v_8}\right\rvert$	0.0089	0.0001	$\left\lvert\frac{\Delta C\alpha - C=O}{\Delta v_8}\right\rvert$	~0	0.002
	$\left\lvert\frac{\Delta M_3}{\Delta v_8}\right\rvert$	0.0179	0.0011	$\left\lvert\frac{\Delta C\beta}{\Delta v_8}\right\rvert$	0.016	0.019
Glu	$\left\lvert\frac{\Delta M_0}{\Delta v_8}\right\rvert$	~0	0.0024	$\left\lvert\frac{\Delta C\alpha}{\Delta v_8}\right\rvert$	0.019	0.018
	$\left\lvert\frac{\Delta M_1}{\Delta v_8}\right\rvert$	0.0006	0.0039	$\left\lvert\frac{\Delta C\alpha - C\beta}{\Delta v_8}\right\rvert$	0.012	0.016
	$\left\lvert\frac{\Delta M_2}{\Delta v_8}\right\rvert$	0.0132	0.0016	$\left\lvert\frac{\Delta C\alpha - C=O}{\Delta v_8}\right\rvert$	~0	0.003
	$\left\lvert\frac{\Delta M_3}{\Delta v_8}\right\rvert$	0.0053	0.0003	$\left\lvert\frac{\Delta C\beta - C\alpha - C=O}{\Delta v_8}\right\rvert$	0.006	0.003
	$\left\lvert\frac{\Delta M_4}{\Delta v_8}\right\rvert$	0.0082	0.0001	$\left\lvert\frac{\Delta C\beta}{\Delta v_8}\right\rvert$	~0	0.016

[a] Sums of squares are as follows: for the GC-MS third-carbon-labeled group, 0.00077; for the GC-MS fully labeled group, 0.00007; for the NMR third-carbon-labeled group, 0.00082; and for the NMR fully labeled group, 0.00128.
[b] Data from the carbon-limited chemostat.
[c] Data from the oxygen-limited chemostat.

NMR data when 10% labeled lactate was used. Coupling NMR analysis with GC-MS could significantly improve the resolution of model calculations when a small fraction of fully labeled substrate is used.

In general, the predicted amino acid isotopomer distributions matched reasonably well with both experimental GC-MS and NMR data (Tables 3 and 4 and Table S2 in the supplemental material), which indicated the accuracy of the model calculation. Besides the instrument errors (GC-MS error, 1 to 2%, and NMR error, 4 to 5%), differences between modeled and measured isotopomer data could arise from other possible sources: (i) errors in the measurement of extracellular fluxes, (ii) background noise from the 1.13% natural abundance of ^{13}C, and (iii) simplification of the model by neglect of the reversibility of less influential pathways. All of the above-mentioned sources complicate the error estimation. An in-depth analysis of the discrepancy between the model-fitting and the experimental data is beyond the scope of this paper.

DISCUSSION

The TCA cycle and serine oxidation pathway (energy production pathways). The TCA cycle was the main carbon metabolism route (with fluxes >60% of lactate uptake), and the flux toward a reversible serine oxidation pathway (PEP to serine to glycine to C_1) was almost 10% of the lactate uptake under carbon-limited conditions. Serine metabolism has often been shown to be reversible in other bacteria (24). But the flux through this pathway (PEP → serine) in MR-1 was much higher than that through the same pathway in *E. coli*, which is 0.9 to 3.5% of the total carbon utilization (43). High flux through serine metabolism suggested that MR-1 is able to oxidize excess C_1. In C_1 metabolism, one ATP and one NADPH are produced when serine is converted to formate via 5,10-Me-THF; an additional NADH is generated when the formate is completely oxidized to CO_2 (10). There are two additional pieces of evidence to support the serine oxidation route. First, high levels of formate dehydrogenase (0.079 μmol/min/mg protein) have been reported for MR-1 under aerobic conditions (26). This enzyme is present in the C_1 oxidation route (Fig. 4). Second, MR-1 can utilize glycine or serine as the sole carbon source when grown in defined medium under aerobic conditions (unpublished data). It would be advantageous for the cell to utilize the serine oxidation pathway to obtain energy (ATP, NADPH, and NADH). The same serine oxidation pathway has also been proposed for *Alteromonas putrefaciens* NCMB 1735 (21).

Under oxygen-limited conditions, the flux through the TCA cycle was reduced (<50%). Scott and Nealson proposed the existence of the serine pathway for MR-1 under anaerobic

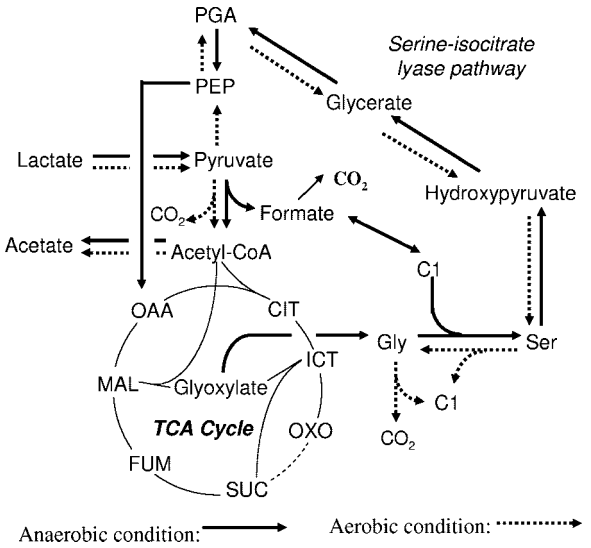

FIG. 4. The proposed serine pathway under anaerobic conditions is shown by the solid arrows. The direction of the serine oxidation pathway under aerobic conditions is shown by the dashed arrows. OAA, oxaloacetate; MAL, malate; OXO, 2-oxoglutarate; PGA, 3-phosphoglycerate; SUC, succinate; CIT, citrate; FUM, fumarate.

conditions (26). This view was established based on high levels of hydroxypyruvate reductase under anaerobic conditions. The fixation of carbon was postulated at the level of formaldehyde, which combines with glycine to yield serine (Fig. 4). Under carbon-limited conditions, the labeling pattern of the α carbon of serine is the same as that of phenylalanine. This observation suggested that the α carbon of serine was derived from the precursor, phosphoenolpyruvate; however, under microaerobic conditions, the labeling pattern of the α carbon of serine is different from that of phenylalanine, and thus, the calculated flux distribution showed another reversible route to produce glycine and serine (glyoxylate → glycine ↔ serine). This proposed pathway is consistent with the reported serine-glyoxylate aminotransferase activity occurring when oxygen is limited (26, 27). However, no significant net flux through the serine pathway (serine → PEP → TCA cycle) was evident under oxygen-limited conditions based on the isotopomer model results.

The pentose phosphate, Entner-Doudoroff, Embden-Meyerhoff-Parnas, and gluconeogenesis pathways. For *E. coli* grown on glucose, the PP pathway flux was over 20% of the total carbon uptake and was utilized mainly for production of reducing equivalents (NADPH) and macromolecule precursors (43). Grown on lactate, the PP pathway flux of MR-1 was very low and used only for biomass production. By comparison of the two chemostat cultures, the average fluxes toward the ED and PP pathways were higher under carbon-limited conditions than under oxygen-limited conditions, because more lactate was used for biomass production under carbon-limited conditions (no acetate production). The ED pathway flux was present in MR-1, consistent with the presence of the active ED pathway enzyme 2-keto-3-deoxygluconate aldolase under aerobic conditions (26). A few bacteria, including *Rhodobacter sphaeroides*, *Sinorhizobium meliloti*, and *Agrobacterium tumefaciens* bacteria, have been shown to substitute the ED pathway for the common EMP pathway (10, 19). These organisms usually lack two essential EMP enzymes, 6-phosphofructokinase and 1,6-biphosphofructoaldolase, which preclude them from using the EMP pathway. MR-1 does not contain phosphofructokinase but appears to contain 1,6-bisphosphofructo-aldolase and fructose-1,6-bisphosphatase (13, 26), which would allow it to synthesize glucose-6-phosphate by using gluconeogenesis. As the Gibbs free energy of reaction suggests that the reaction of glucose-6-phosphate to 6-phosphogluconate is unidirectional (39), the reverse EMP pathway instead of the ED pathway is the only possible route for synthesizing the carbohydrate precursor glucose-6-phosphate.

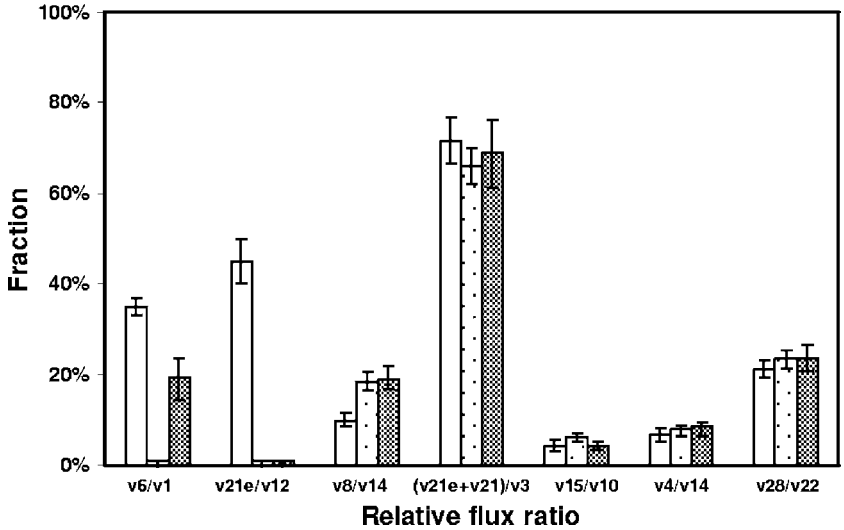

FIG. 5. Relative flux ratios in the central metabolic pathways under carbon-limited chemostat, oxygen-limited chemostat, and shake flask cultures. The flux ratio represents the relative relationships between key metabolic routes. v6/v1, acetate production; v21e/v12, serine-glyoxylate aminotransferase; v8/v14, malate synthase/TCA; (v21+v21e)/v3, serine metabolism/glycolysis; v15/v10, glyoxylate shunt/TCA; v4/v14, phosphoenolpyruvate synthase/TCA; ED pathway/glycolysis. Empty bars, oxygen limited; stippled bars, carbon limited; filled bars, shake flask culture.

Futile cycles. Two anaplerotic reactions appeared to be present (pyruvate to malate, catalyzed by malate dehydrogenase, and oxaloacetate to phosphoenolpyruvate, catalyzed by phosphoenolpyruvate carboxykinase) and formed a futile cycle. In a previous study, malate dehydrogenase and phosphoenolpyruvate carboxylase of MR-1 were shown to be active under aerobic conditions (26). In this study, the pyruvate-to-malate flux was around 13% of the lactate uptake under the carbon-limited condition and less than half this value under the oxygen-limited condition. A similar change in flux was also observed in the oxaloacetate-to-phosphoenolpyruvate reaction under the two chemostat conditions.

Highly coupled to the anaplerotic reactions (via malate) is the glyoxylate shunt. The flux through the glyoxylate shunt was below 4% of the lactate uptake rate under both chemostat conditions. This finding correlated with the reported lower level (0.009 μmol/min/mg protein) of isocitrate lyase activity than for other TCA cycle-related enzymes (26). The glyoxylate shunt is necessary for synthesizing TCA cycle intermediates, such as succinate and malate, and is also an important step for the serine pathway (isocitrate to glyoxylate to glycine) proposed for MR-1 under oxygen-limited conditions.

There appears to be a futile cycle involving the reactions pyruvate → malate, malate → oxaloacetate, and oxaloacetate → phosphoenolpyruvate. It is not clear why the cell would choose to route flux through this circuitous pathway rather than directly through the reaction pyruvate → phosphoenolpyruvate. These pathways might help to increase the flexibility in central carbon metabolism, to allow MR-1 to utilize different electron acceptors, or to maintain stability in central metabolism under environmental stresses (3, 34).

Flux ratio analysis and verification of model results. From GC-MS data (Table 3), the isotopomer distributions of key amino acids obtained from shake flask cultures were relatively similar to those from chemostat cultures. However, based on the isotopomer data from the shake flask cultures (using third-position-labeled lactate), the fluxes through the TCA cycle and the reactions that transform acetyl-CoA to acetate were calculated to be 48% and 19% of the lactate consumption, respectively. These values were very different from those obtained from either the carbon-limited or the oxygen-limited chemostat cultures. As the shake flask culture is non-steady state, the oxygen concentration changes from fully aerobic to microaerobic (31). It is known that the relative flux ratios rather than the absolute fluxes in key pathways determine the isotopomer distribution (23). The metabolic flux ratios for key pathways were analyzed to reveal the similarity in the flux distribution of the central metabolism under the two chemostat and shake flask conditions (Fig. 5). Although acetate production, growth rate, and most intracellular fluxes were very different under these three conditions, many flux ratios in the TCA cycle and futile cycles did not differ significantly (the difference between the ratios for the carbon-limited chemostat and the shake flask culture was below 5%). The same invariability in the flux ratios was also found in *Bacillus subtilis* and *E. coli* (7, 23). This observation suggests that central metabolism in some microorganisms is under specific regulation and is robust to environmental changes (28). Even though the shake flask culture conditions were not identical to those of the chemostat cultures, the robust nature of bacterial metabolism helps to maintain their relative flux ratios. This supports the idea that shake flask cultures may sometimes substitute for continuous culture for metabolic flux analysis, at least to obtain a reliable measurement of central metabolic flux ratios (23).

As our study showed that the isotopomer distributions in *S. oneidensis* MR-1 were not sensitive to culture methods under the aerobic condition, analyzing the isotopomer distributions from shake flasks with differently labeled lactate substrates is an efficient and reliable approach for checking the accuracy of the flux estimations from chemostat cultures. First, using 99% [1-^{13}C]L-lactate as the carbon source, the model used the flux

TABLE 6. Results for flux distribution reliability test: predicted and measured fragment mass $[M-57]^+$ distributions of key amino acids when 1-^{13}C-labeled lactate medium was used for shake flask culture ($n = 2$)[a]

Related pathway, amino acid, and ion (m/z)	Model prediction	Measured value
Pyruvate synthesis route		
Ala		
M0	0.02	0.03 ± 0.01
M1	0.98	0.98 ± 0.01
M2	0	0 ± 0
Val		
M0	0.02	0.05 ± 0.01
M1	0.96	0.94 ± 0.01
M2	0	0 ± 0
Serine oxidation route		
Ser		
M0	0.24	0.21 ± 0.03
M1	0.76	0.79 ± 0.03
M2	0.0	0 ± 0
Gly		
M0	0.25	0.34 ± 0.03
M1	0.75	0.66 ± 0.03
M2	0	0 ± 0
TCA cycle		
Asp		
M0	0.78	0.75 ± 0.04
M1	0.12	0.14 ± 0.02
M2	0.10	0.10 ± 0.01
Glu/Gln		
M0	0.89	0.86 ± 0.03
M1	0.09	0.07 ± 0.02
M2	0.01	0.03 ± 0.02
PP pathway		
Phe		
M0	0.01	0.01 ± 0
M1	0.13	0.09 ± 0.03
M2	0.42	0.36 ± 0.05
M3	0.42	0.52 ± 0.08
His		
M0	0.23	0.18 ± 0.05
M1	0.76	0.75 ± 0.06
M2	0.01	0.04 ± 0.02

[a] The flux rate distribution listed in Fig. 3 (for the carbon-limited condition) was used for model prediction.

distribution from the carbon-limited conditions to predict the isotopomer distribution of six key amino acids. The model prediction was then compared with the experimental isotopomer distribution obtained from the culture grown aerobically in shake flasks containing 30 mM 99% [1-^{13}C]L-lactate. The accuracy of the flux estimation was validated since the experimental isotopomer data were consistent with the model predictions (Table 6).

GC-MS and NMR measurements of isotopomer distributions in proteinogenic amino acids, the annotated genome, and mathematical algorithms enabled us to develop a metabolic pathway model to quantify the intracellular fluxes of the central metabolic pathways. The results revealed a general metabolic flux distribution under both carbon-limited and oxygen-limited conditions. Our study also identified several active pathways, including a potential futile cycle, the ED pathway, the serine oxidation pathway, and the activity of serine-glyoxylate aminotransferase (under microaerobic conditions). Furthermore, this research demonstrates successful applications of NMR and GC-MS for metabolic flux analysis, particularly where small fractions of fully labeled substrates were used.

ACKNOWLEDGMENTS

We thank Jim Fredrickson, Yuri Gorby, and Grigoriy Pinchuk (Pacific Northwest National Laboratory, Richland, WA) for advice on culturing MR-1. We also thank Adam Meadows, Farnaz Nowroozi, Kenny Tran, and Kishen Guna (University of California—Berkeley) for helping with experiments and isotopomer modeling.

This work is part of the Virtual Institute for Microbial Stress and Survival (http://VIMSS.lbl.gov), supported by the U.S. Department of Energy, Office of Science, Office of Biological and Environmental Research, Genomics:GTL Program, through contract DE-AC02-05CH11231 between the Lawrence Berkeley National Laboratory and the U.S. Department of Energy.

REFERENCES

1. **Alm, E. J., K. H. Huang, M. N. Price, R. P. Koche, K. Keller, I. L. Dubchak, and A. P. Arkin.** 2005. The MicrobesOnline Web site for comparative genomics. Genome Res. **15:**1015–1022.
2. **Arauzo-Bravo, M. J., and K. Shimizu.** 2003. An improved method for statistical analysis of metabolic flux analysis using isotopomer mapping matrices with analytical expressions. J. Biotechnol. **105:**117–133.
3. **Christiansen, T., B. Christensen, and J. Nielsen.** 2002. Metabolic network analysis of *Bacillus claussi* on minimal and semirich medium using ^{13}C-labeled glucose. Metab. Eng. **4:**159–169.
4. **Daniels, L., R. S. Hanson, et al.** 1994. Chemical analysis, p. 512–554. *In* P. Gerhardt, R. Murray, W. Wood, and N. Krieff (ed.), Methods for general and molecular bacteriology. American Society for Microbiology, Washington, DC.
5. **Delaglio, F., S. Grzesiek, G. Vuister, G. Zhu, J. Pfeifer, and A. Bax.** 1995. NMR pipe: a multidimensional spectral processing system based on UNIX pipes. J. Biomol. NMR **6:**277–293.
6. **Dookeran, N. N., T. Yalcin, and A. G. Harrison.** 1996. Fragmentation reactions of protonated α-amino acids. J. Mass Spectrom. **31:**500–508.
7. **Fischer, E., and U. Sauer.** 2005. Large-scale *in vivo* flux analysis shows rigidity and suboptimal performance of *Bacillus subtilis* metabolism. Nat. Genet. **37:**636–640.
8. **Fischer, E., and U. Sauer.** 2003. Metabolic flux profiling of *Escherichia coli* mutants in central carbon metabolism using GC-MS. Eur. J. Biochem. **270:** 880–891.
9. **Fischer, E., N. Zamboni, and U. Sauer.** 2004. High-throughput metabolic flux analysis based on gas chromatography-mass spectrometry derived 13C constraints. Anal. Biochem. **325:**308–316.
10. **Fuhrer, T., E. Fischer, and U. Sauer.** 2005. Experimental identification and quantification of glucose metabolism in seven bacterial species. J. Bacteriol. **187:**1581–1590.
11. **Ghosal, D., M. Omelchenko, E. Gaidamakova, V. Matrosova, A. Vasilenko, A. Venkateswaran, M. Zhai, H. Kostandarithes, H. Brim, K. Makarova, L. Wackett, J. Fredrickson, and M. Daly.** 2005. How radiation kills cells: survival of Deinococcus radiodurans and Shewanella oneidensis under oxidative stress. FEMS Microbiol. Rev. **29:**361–375.
12. **Harrison, A. G.** 2001. Ion chemistry of protonated glutamic acid derivatives. Int. J. Mass Spectrom. **210/211:**361–370.
13. **Heidelberg, J. F., I. T. Paulsen, I. T. Nelson, E. J. Gaidos, W. C. Nelson, T. D. Read, J. A. Eisen, R. Seshadri, N. Ward, B. Methe, R. A. Clayton, T. Meyer, A. Tsapin, J. Scott, M. Beanan, L. Brinkac, S. Daugherty, R. T. DeBoy, R. J. Dodson, A. S. Durkin, D. H. Haft, J. F. Kolonay, R. Madupu, J. D. Peterson, L. A. Umayam, O. White, A. M. Wolf, J. Vamathevan, J. Weidman, M. Impraim, K. Lee, K. Berry, C. Lee, J. Mueller, H. Khouri, J. Gill, T. R. Utterback, L. A. McDonald, T. V. Feldblyum, H. O. Smith, J. C. Venter, K. H. Nealson, and C. M. Fraser.** 2002. Genome sequence of the dissimilatory metal-ion reducing bacterium Shewanella oneidensis. Nat. Biotechnol. **20:**1118–1123.
14. **Hellerstein, M. K., and R. A. Neese.** 1999. Mass isotopomer distribution analysis at eight years: theoretical, analytic, and experimental considerations. Am. J. Physiol. Endocrinol. Metab. **276:**E1146–E1170.
15. **Herbert, D., P. J. Phipps, et al.** 1971. Chemical analysis of microbial cells, p. 210–344. *In* J. R. Norris and D. W. Ribbons (ed.), Methods in microbiology, vol. 5B. Academic Press, Inc., New York, NY.
16. **Marshal, J.** 2004. Production of secondary metabolites from acetyl Co-A precursors in bacterial and fungal hosts. Ph.D. thesis. University of California, Berkeley.
17. **Middleton, S. S., R. B. Latmani, M. R. Mackey, M. H. Ellisman, B. M. Tebo, and C. S. Criddle.** 2003. Cometabolism of Cr(VI) by *Shewanella oneidensis* MR-1 produces cell-associated reduced chromium and inhibits growth. Biotechnol. Bioeng. **83:**627–637.
18. **Neal, A. L., K. Lowe, T. L. Daulton, J. Jones-Meehan, and B. J. Little.** 2002. Oxidation state of chromium associated with cell surfaces of *Shewanella oneidensis* during chromate reduction. Appl. Surf. Sci. **202:**150–159.
19. **Nicklin, J., K. Graeme-Cook, T. Paget, and R. A. Killington.** 1999. Instant notes in microbiology. Bios Scientific Publishers, London, United Kingdom.
20. **Press, W. H., S. A. Teukolsky, W. T. Vetterling, and B. P. Flannery.** 1992. Numerical recipes in FORTRAN, 2nd ed. Cambridge University Press, Cambridge, United Kingdom.
21. **Ringo, E. E., E. Stenberg, and A. R. Strom.** 1984. Amino acid and lactate catabolism in trimethylamine oxide respiration of *Alteromonas putrefaciens* NCMB 1735. Appl. Environ. Microbiol. **47:**1084–1089.
22. **Sauer, U.** 2004. High-throughput phenomics: experimental methods for mapping fluxomes. Curr. Opin. Biotechnol. **15:**58–63.
23. **Sauer, U., D. R. Lasko, J. Fiaux, M. Hochuli, R. Glaser, T. Szyperski, K. Wuthrich, and J. E. Bailey.** 1999. Metabolic flux ratio analysis of genetic and environmental modulations of *Escherichia coli* central carbon metabolism. J. Bacteriol. **181:**6679–6688.
24. **Schmidt, K., J. Nielsen, and J. Villadsen.** 1999. Quantitative analysis of metabolic fluxes in *Escherichia coli*, using two-dimensional NMR spectroscopy and complete isotopomer models. J. Biotechnol. **71:**175–190.
25. **Schmidt, K., L. C. Norregaard, B. Pedersen, A. Meissner, and J. Q. Nielsen.** 1999. Quantification of intracellular metabolic fluxes from fractional enrichment and ^{13}C-^{13}C coupling constraints on the isotopomer distribution in labeled biomass components. Metab. Eng. **1:**166–179.
26. **Scott, J. H., and K. H. Nealson.** 1994. A biochemical study of the intermediary carbon metabolism of *Shewanella putrefaciens*. J. Bacteriol. **176:**3408–3411.
27. **Serres, M. H., and M. Riley.** 2006. Genomic analysis of carbon source metabolism of *Shewanella oneidensis* MR-1: predictions versus experiments. J. Bacteriol. **188:**4601–4609.
28. **Stelling, J., U. Sauer, Z. Szallasi, F. Doyle, and J. Doyle.** 2004. Robustness of cellular functions. Cell **118:**675–685.
29. **Stephanopoulos, G. N., A. A. Aristidou, and J. Nielsen.** 1998. Metabolic engineering principles and methodologies. Academic Press, San Diego, CA.
30. **Szyperski, T.** 1995. Biosynthetically directed fractional ^{13}C labeling of proteinogenic amino acids: an efficient analytical tool to investigate intermediary metabolism. Eur. J. Biochem. **232:**433–448.
31. **Tang, Y. J., D. Laidlaw, K. Gani, and J. D. Keasling.** 2006. Evaluation of the effects of various culture conditions on Cr(VI) reduction by *Shewanella oneidensis* MR-1 in a novel high-throughput mini-bioreactor. Biotechnol. Bioeng. **95:**176–184.
32. **Tang, Y. J., A. L. Meadows, and J. D. Keasling.** 2006. A kinetic model describing *Shewanella oneidensis* MR-1 growth, substrate consumption, and product secretion. Biotechnol. Bioeng. **96:**125–133.
33. **Teece, M. A., M. L. Fogel, M. E. Dollhopf, and K. H. Nealson.** 1999. Isotopic fraction associated with biosynthesis of fatty acids by a marine bacterium under oxic and anoxic conditions. Org. Geochem. **30:**1571–1579.
34. **Tiedje, J.** 2002. Shewanella—the environmentally versatile genome. Nat. Biotechnol. **20:**1093–1094.
35. **Venkateswaran, K., D. P. Moser, M. E. Dollhopf, D. P. Lies, D. A. Saffarini, B. J. MacGregor, D. B. Ringelberg, D. C. White, M. Nishijima, H. Sano, J. Burghardt, E. Stackebrandt, and K. H. Nealson.** 1999. Polyphasic taxonomy of the genus *Shewanella* and description of *Shewanella oneidensis sp*. Int. J. Syst. Bacteriol. **49:**705–724.
36. **Viamajala, S., B. M. Peyton, W. A. Apel, and J. N. Petersen.** 2002. Chromate/nitrite interactions in *Shewanella oneidensis* MR-1: evidence for multiple hexavalent chromium [Cr(VI)] reduction mechanisms dependent on physiological growth conditions. Biotechnol. Bioeng. **78:**770–778.

37. **Viamajala, S., B. M. Peyton, R. K. Sani, W. A. Apel, and J. N. Petersen.** 2004. Toxic effect of chromium(VI) on anaerobic and aerobic growth of *Shewanella oneidensis* MR-1. Biotechnol. Prog. **20:**87–95.
38. **Wiechert, W.** 2001. ^{13}C metabolic flux analysis. Metab. Eng. **3:**195–206.
39. **Wiechert, W., and A. A. de Graaf.** 1997. Bidirectional reaction steps in metabolic networks: I. Modeling and simulation of carbon isotope labeling experiments. Biotechnol. Bioeng. **55:**101–117.
40. **Wiechert, W., M. Mollney, S. Petersen, and A. A. de Graaf.** 2001. A universal framework for ^{13}C metabolic flux analysis. Metab. Eng. **3:**265–283.
41. **Wiechert, W., C. Siefke, A. A. de Graaf, and A. Marx.** 1997. Bidirectional reaction steps in metabolic networks: II. Flux estimation and statistical analysis. Biotechnol. Bioeng. **55:**118–135.
42. **Zhang, C. L., Y. Li, Q. Ye, J. Fong, A. D. Peacock, E. Blunt, J. Fang, D. R. Lovley, and D. C. White.** 2003. Carbon isotope signatures of fatty acids in *Geobacter metallireducens* and *Shewanella algae*. Chem. Geol. **195:**17–28.
43. **Zhao, J., and K. Shimizu.** 2003. Metabolic flux analysis of *Escherichia coli* K12 grown on 13C-labeled acetate and glucose using GC-MS and powerful flux calculation method. J. Biotechnol. **101:**101–117.